Large antenna array and propagation environment interaction

Gao, Xiang; Zhu, Meifang; Rusek, Fredrik; Tufvesson, Fredrik; Edfors, Ove

Published in:
Proc. 48th Asilomar Conference on Signals, Systems and Computers, ACSSC 2015

DOI:
10.1109/ACSSC.2014.7094530

2014

Large antenna array and propagation environment interaction

Xiang Gao, Meifang Zhu, Fredrik Rusek, Fredrik Tufvesson, Ove Edfors
Department of Electrical and Information Technology, Lund University, Sweden
Email: {xiang.gao, meifang.zhu, fredrik.rusek, fredrik.tufvesson, ove.edfors}@eit.lth.se

***Abstract*—In conventional MIMO, propagation conditions are often considered wide-sense stationary over the entire antenna array. In massive MIMO systems, where arrays can span over large physical dimensions, the situation is quite different. For instance, significant variations in signal strength, due to shadowing, can be experienced across a large array. These effects vary with propagation environment in which the array is placed, and influence achievable sum-rates. We characterize these variations for several measured propagation scenarios in the 2.6 GHz frequency range and illustrate how power variations and correlation properties change along the array.**

***Index Terms*—massive MIMO, channel measurements, spatial correlation, Kronecker model, Toeplitz structure, sum-rate**

I. Introduction

In conventional multi-user MIMO (MU-MIMO) where a base station is equipped with a relatively small number of antennas, the propagation properties are often considered stationary over the entire array. In this case the fading and spatial correlation properties across the array are characterized by a Toeplitz-structured correlation matrix [1] [2].

When conventional MIMO is scaled up to massive MIMO [3] [4], however, the situation becomes different. The propagation properties, *i.e.*, channel strength and spatial correlation among antenna elements, may vary significantly over large arrays. Arrays that span large physical dimensions, or directional patterns of the array antenna elements, can be the source of these variations [5]–[7]. These variations in channel strength and spatial correlation play an important role for massive MIMO performance. For instance, large-scale fading can be experienced on large arrays due to shadowing effects, which makes antenna elements contribute unequally to the system performance. The spatial correlation between antenna elements can degrade the ability of massive MIMO to decorrelate users. Variation in spatial correlation on a large array leads to some antenna element combinations performing better than others. For accurate simulation of massive MIMO systems, these fading and correlation properties on large arrays should be considered and included in massive MIMO channel models. The Toeplitz structure used for small arrays, therefore, may not be suitable.

Here we illustrate fading and correlation properties on large arrays when they interact with different propagation environments. The investigations are based on measured channels in the 2.6 GHz frequency range, using a virtual linear array and a patch cylindrical array, both having 128 elements. The linear array spans a large physical dimension in space, while the cylindrical array is relatively small in size. For the linear array, we compare its fading and spatial correlation structure with the Toeplitz structure. Specifically, we apply the measured structure and the Toeplitz structure in the Kronecker model [8] [9], and compare their achievable sum-rates. The Kronecker model is by far the most popular MIMO channel model, mainly due to its simplicity and analytical tractability [10]. However, it is based on the assumption that scattering around the transmitter can be separated from scattering around the receiver. For example, when the transmitter and receiver are separated by a large distance, the correlation properties on both sides may be dominated by scatterers in the immediate vicinity of the transmitter and receiver. If the transmit and receive correlation are coupled somehow, studies have shown that the Kronecker model will underestimate the channel capacity [11]. Therefore, in our study, the sum-rates achieved in the measured channels are shown as a reference, and compared with those obtained by assuming a Kronecker model, where the correlation across the large array is modeled either with or without an additional Toeplitz-structure assumption. This comparison can reveal how well the Kronecker and Toeplitz structure assumptions on channel correlation match the real channels on which they are based. For the cylindrical array, the variation in channel strength and correlation is due to its patch antenna patterns and circular arrangement, rather than fading and spatial correlation in the propagation channels. This makes the fading and correlation structure on this array naturally different from the Toeplitz structure.

The rest of the paper is organized as follows. In Sec. II we describe the channel measurements. In Sec. III we describe our system model, and the Kronecker model with both measured and Toeplitz-structured correlation matrices. Then in Sec. IV we illustrate the fading and correlation properties on the large arrays, and present the comparison results of the sum-rates achieved. Finally we summarize this work in Sec. V.

II. Measured channels

The massive MIMO channel measurements used in this analysis have been reported in [5] and [6]. Here we briefly describe the two large arrays and the measured channels.

The measured channels were obtained from two measurement campaigns performed with two different large arrays at the base station. Both arrays contain 128 antenna elements and have an adjacent element spacing of half a wavelength at 2.6 GHz. Fig. 1a shows the cylindrical array, having 16 dual-polarized directional patch antennas in each circle and 4 such circles stacked on top of each other, which gives a total of 128 antenna ports. This array has both diameter and height around 30 cm. Fig. 1b shows the virtual linear array with a

a) Cylindrical array b) Virtual linear array

Fig. 1. Two large arrays: a) a cylindrical array with 64 dual-polarized patch antenna elements, giving 128 ports in total, and b) a virtual linear array with 128 vertically-polarized omni-directional antennas.

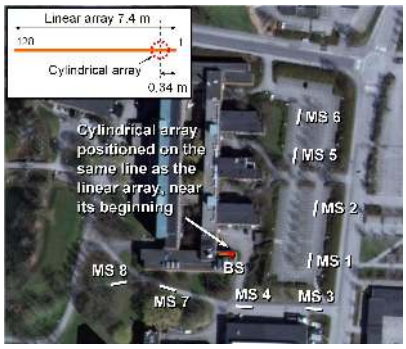

Fig. 2. Overview of the measurement area at the campus of Lund University, Sweden. The two large arrays were placed on the roof of the E-building during two campaigns. Eight sites (MS 1-8) around the E-building were measured.

vertically-polarized omni-directional antenna moving along a rail, in 128 equidistant positions. In comparison, the linear array spans 7.4 m in space, which is more than 20 times the size of the cylindrical array. In both measurements, an omni-directional antenna with vertical polarization was used at the user side. Measurement data were recorded at center frequency 2.6 GHz and a signal bandwidth of 50 MHz.

Both measurements were performed outdoors at the E-building of the Faculty of Engineering (LTH), Lund University, Sweden. Fig. 2 gives an overview of the measurement area. The two arrays were placed on the same roof of the E-building during their respective measurement campaigns. More precisely, the cylindrical array was positioned on the same line as the linear array, near its beginning. At the user side, the omni-directional antenna was moved around the E-building at 8 measurement sites (MS), acting as single-antenna users. Among these sites, three (MS 1-3) have line-of-sight (LOS) conditions, and four (MS 5-8) have non-line-of-sight (NLOS) conditions, while one (MS 4) has LOS for the cylindrical array, but the LOS component is blocked by the roof edge for the linear array. At each site, with the cylindrical array, we measured five parallel stretches of 40 points giving a total of 200 positions, while with the linear array, 5 positions within 5 m were measured.

III. System description

We assume multi-user MIMO-OFDM transmission with M base station antennas, K users, and L subcarriers. The uplink transmission at subcarrier ℓ is

$$\boldsymbol{y}_\ell = \boldsymbol{H}_\ell^T \boldsymbol{s}_\ell + \boldsymbol{n}_\ell, \tag{1}$$

where $\boldsymbol{H}_\ell$ of size $K \times M$ is the propagation matrix at subcarrier ℓ, $\boldsymbol{s} = [s_1\ s_2\ \ldots\ s_K]^T$ is a $K \times 1$ vector, and s_i is a complex data symbol transmitted by the ith user with averaged energy $\mathbb{E}\left\{|s_i|^2\right\} = E_{s,i}$, $\boldsymbol{n}_\ell$ is the complex Gaussian noise vector with variance N_0 in each element.

Assuming that all users have the same transmit energy which is reduced with the number of base station antennas, *i.e.*, $E_{s,i} = E_s/M$, the uplink sum-rate at subcarrier ℓ is [12]

$$C_{\text{uplink},\ell} = \log_2 \det \left(\boldsymbol{I}_M + \frac{E_s}{N_0 M} \boldsymbol{H}_\ell^H \boldsymbol{H}_\ell \right). \tag{2}$$

The reason to decrease the transmit energy with M is that we would like to harvest the increasing array gain at the base station as reduced transmit power from each user.

The fading and correlation on base station antenna array, at subcarrier ℓ, can be described by the $M \times M$ Gram matrix

$$\boldsymbol{R}_{\text{BS},\ell} = \boldsymbol{H}_\ell^H \boldsymbol{H}_\ell, \tag{3}$$

where the diagonal element $[\boldsymbol{R}_{\text{BS},\ell}]_{m,m}$ shows the combined strength of the channels from antenna m to all K users, and the off-diagonal element $[\boldsymbol{R}_{\text{BS},\ell}]_{m_1,m_2}$ measures the spatial dependency between antenna m_1 and m_2 by the inner product of the two channel vectors. Shadow fading across the array can be seen as variations on the diagonal, while spatial correlation is captured by the off-diagonal elements.

From the correlation matrix $\boldsymbol{R}_{\text{BS},\ell}$, we estimate a Toeplitz matrix in a least-square sense. We first obtain the averaged correlation γ_ℓ as a function of the antenna separation Δ,

$$\gamma_\ell(\Delta) = \frac{1}{M-\Delta} \sum_{m=1}^{M-\Delta} [\boldsymbol{R}_{\text{BS},\ell}]_{m,m+\Delta}, \tag{4}$$

where $0 \le \Delta \le M-1$. Then, we structure the Toeplitz matrix as

$$\boldsymbol{T}_{\text{BS},\ell} = \begin{bmatrix} \gamma_\ell(0) & \gamma_\ell(1) & \gamma_\ell(2) & \cdots & \gamma_\ell(M-1) \\ \gamma_\ell^*(1) & \gamma_\ell(0) & \gamma_\ell(1) & \ddots & \vdots \\ \gamma_\ell^*(2) & \gamma_\ell^*(1) & \ddots & \ddots & \vdots \\ \vdots & \ddots & \ddots & \ddots & \gamma_\ell(1) \\ \gamma_\ell^*(M-1) & \cdots & \cdots & \gamma_\ell^*(1) & \gamma_\ell(0) \end{bmatrix}. \tag{5}$$

The Toeplitz structure assumes no shadow fading and no variation in spatial correlation across the array.

In order to compare the measured correlation and Toeplitz-structured correlation in terms of achievable sum-rate, we apply $\boldsymbol{R}_{\text{BS},\ell}$ and $\boldsymbol{T}_{\text{BS},\ell}$ in the Kronecker model. We have

$$\boldsymbol{H}_{\text{Kron},\ell}^{\text{Meas}} = \boldsymbol{H}_{\text{iid},\ell} \left(\boldsymbol{R}_{\text{BS},\ell}^{1/2} \right)^T \tag{6}$$

and

$$\boldsymbol{H}_{\text{Kron},\ell}^{\text{Toep}} = \boldsymbol{H}_{\text{iid},\ell} \left(\boldsymbol{T}_{\text{BS},\ell}^{1/2} \right)^T, \tag{7}$$

where $\boldsymbol{H}_{\text{iid},\ell}$ is a $K \times M$ matrix with independent and identically distributed (i.i.d.) complex Gaussian coefficients. Note that we assume user-side correlation to be an identity matrix, *i.e.*, user channels are orthogonal and have no difference in propagation loss. By replacing $\boldsymbol{H}_\ell$ in (2) with $\boldsymbol{H}_{\text{Kron},\ell}^{\text{Meas}}$ or $\boldsymbol{H}_{\text{Kron},\ell}^{\text{Toep}}$, we have the corresponding sum-rate for one channel realization of the Kronecker model at subcarrier ℓ. By generating N realizations of the i.i.d. channel, we obtain

the average sum-rate of all realizations at subcarrier ℓ, and then make comparisons between the measured correlation and the Toeplitz-structured correlation. Note that when calculating the sum-rate, both the channel matrix $\boldsymbol{H}_{\mathrm{Kron},\ell}^{\mathrm{Meas}}$ and $\boldsymbol{H}_{\mathrm{Kron},\ell}^{\mathrm{Toep}}$ are normalized to have the same norm as $\boldsymbol{H}_{\ell}$.

Next, we apply the measured channels in our system model, and illustrate the fading and correlation properties on the large arrays in different propagation environments.

IV. Fading and correlation properties

We first present the results with the linear array, as it characterizes the variation of propagation conditions in large spatial dimensions. Then we turn to the compact cylindrical array, which experiences only a small part of the channel "seen" by the much larger linear array.

A. Linear array

We choose three scenarios to study and make comparisons: two LOS scenarios, MS 1 and MS 3, and one NLOS scenario, MS 5. For an intuitive understanding of the propagation condition in each scenario, we show the angular power spectrum along the linear array, estimated by a 10-antenna sliding window using the Minimum Variance Method (MVM) [13], as in Fig. 3(a), 5(a) and 7(a). For each scenario, we show the averaged fading and correlation matrix over $L = 161$ subcarriers, *i.e.*, $\frac{1}{L}\sum_{\ell=1}^{L}|\boldsymbol{R}_{\mathrm{BS},\ell}|$, in Fig. 3(b), 5(b) and 7(b). The reason for averaging over the absolute values is that the phase difference between subcarriers does not help decorrelate the antenna elements, as subcarriers are independent "sub-channels" in OFDM. Then in Fig. 3(c), 5(c) and 7(c), we illustrate the averaged channel strength over subcarriers along the array, which is basically the diagonal elements in the fading and correlation matrix. For the off-diagonal elements, we extract the correlation coefficient with respect to the antenna separation in wavelength, and show the averaged correlation coefficient over subcarriers in Fig. 3(d), 5(d) and 7(d).

In order to measure the difference of the measured and the Toeplitz-structured correlation, in Fig. 4, 6 and 8, we compare the uplink sum-rates achieved by the Kronecker model with the two correlation matrices. The sum-rate achieved in the measured channels is shown as a reference. We have $K = 5$ users and show the cases of 5, 32, 64 and 128 base station antennas. Antennas are selected adjacent to each other on the linear array, representing the situation of smaller arrays. We randomly generate $N = 100$ realizations of the i.i.d. channel, and the sum-rates are averaged over different selections of the smaller arrays, i.i.d. channel realizations and subcarriers. We investigate the difference of the measured and the Toeplitz-structured correlation with respect to the array size.

Now we turn attention to the LOS scenario where the users are at MS 1. The LOS component is from the array end-fire direction, as can be seen in Fig. 3(a), and the incoming energy concentrates at 0 and 180 degrees due to the estimation error for the end-fire direction with the linear array structure. Despite this, we see how the angular power spectrum varies along the array. The energy is stronger at the beginning of the array, and some energy from scatterers around 150 degrees

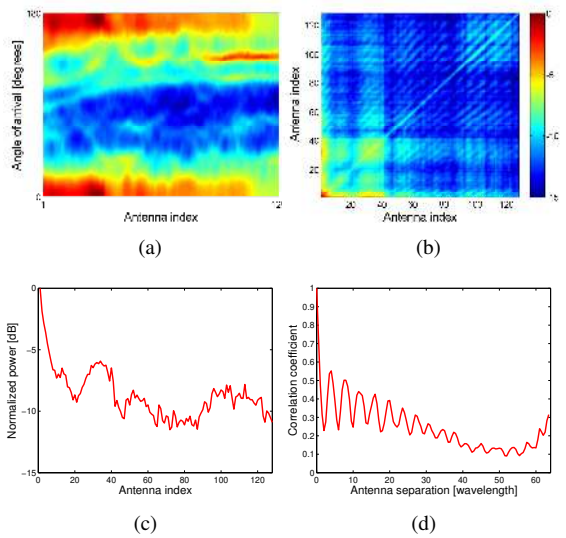

Fig. 3. A LOS scenario where five users are at MS 1. (a) Angular power spectrum along the linear array. (b) Averaged fading and correlation over subcarriers on the array. (c) Variation in channel strength across the array. (d) Averaged spatial correlation with respect to antenna separation.

appears at the end. Correspondingly, in Fig. 3(b) that shows the averaged fading and correlation matrix, the income energy is stronger at antennas 1-40, and becomes weaker at the rest part of array. This can also be seen in Fig. 3(c) that the variation in channel strength is more than 10 dB along the array. In Fig. 3(d), we observe ripples in the averaged correlation coefficient with respect to the antenna separation. This is because the end-fire direction of the LOS component causes a rapid phase rotation along the array. At around 50 wavelengths the correlation coefficient reduces to 0.1.

Comparing the measured correlation along the array with the Toeplitz structure in terms of achievable sum-rate, we see in Fig. 4 that the Kronecker model with the Toeplitz-structured correlation gives higher sum-rates, for all the cases of 5, 32, 64 and 128 antennas, especially at high E_s/N_0. At low E_s/N_0, the difference in sum-rates is very small. At high E_s/N_0, *e.g.*, 10 dB, the Kronecker model with the Toeplitz-structured correlation achieves 10%, 25%, 28% and 32% higher sum-rate than the model with the measured correlation, for 5, 32, 64 and 128 antennas, respectively. As expected, when the array size grows larger, the measured fading and correlation becomes more different with the Toeplitz structure.

When comparing the sum-rate achieved in the Kronecker model with that achieved in the measured channels, we observe that the Kronecker model with the measured correlation underestimates the sum-rate. At $E_s/N_0 = 10$ dB, the sum-rate by the Kronecker model is 9%, 15%, 16% and 18% lower than that achieved in the measured channels, for 5, 32, 64 and 128 antennas, respectively. It indicates that the Kronecker model underestimates the sum-rate to a larger extent for larger arrays. We also observe that the sum-rate obtained by the Kronecker model with the Toeplitz correlation is closer to the measured sum-rate. This is because that the Toeplitz structure wins back the degradation introduced by the Kronecker model. This, however, does not mean that the Toeplitz structure is

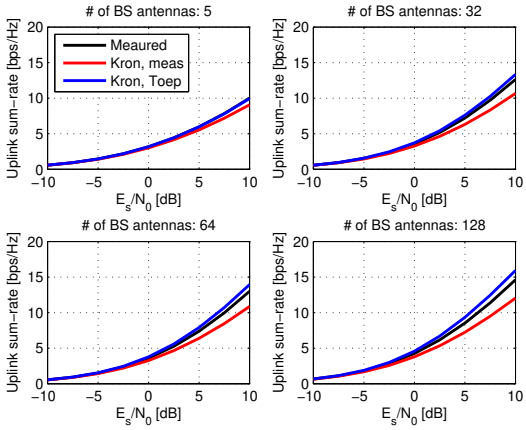

Fig. 4. Comparison of the sum-rates achieved in the measured channels, and in the Kronecker model with the measured and the Toeplitz correlation. The users are at MS 1, all having LOS conditions.

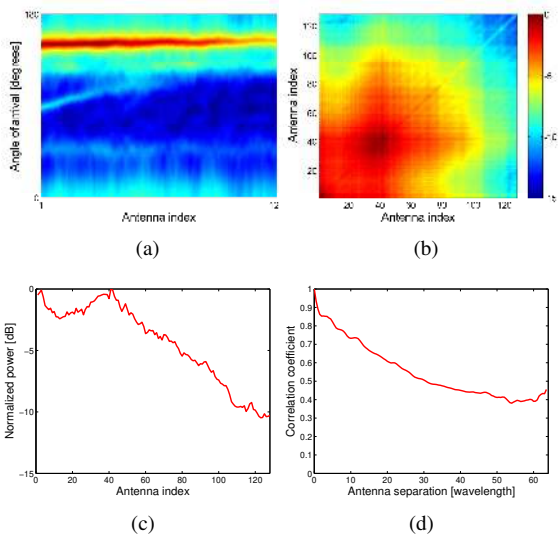

Fig. 5. A LOS scenario where five users are at MS 3. (a) Angular power spectrum along the linear array. (b) Averaged fading and correlation over subcarriers on the array. (c) Variation in channel strength across the array. (d) Averaged spatial correlation with respect to antenna separation.

suitable for the fading and correlation on large arrays.

We move on to another LOS scenario where the users are at MS 3. In Fig. 5(a), we see a clear LOS component from around 160 degrees along the entire array. The LOS component is stronger at the beginning of the array, and gradually becomes shadowed. This shadowing effect can be seen in the fading and correlation matrix in Fig. 5(b). Fig. 5(c) shows that the variation in channel strength is more than 10 dB. In Fig. 5(d), we see a higher spatial correlation than in the previous scenario, which is due to the stronger LOS component. In this case the correlation coefficient only goes down to about 0.4.

In Fig. 6, the Toeplitz structure again gives higher sum-rates than the measured correlation. At $E_s/N_0 = 10$ dB, the sum-rate obtained by the Kronecker model with the Toeplitz-structured correlation is 10%, 20%, 23% and 28% higher than that obtained with the measured correlation, for 5, 32, 64 and 128 antennas, respectively. It means that for larger

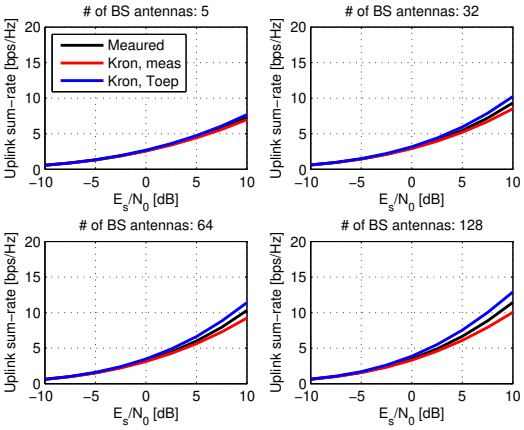

Fig. 6. Comparison of the sum-rates achieved in the measured channels, and in the Kronecker model with the measured and the Toeplitz correlation. The five users are at MS 3, all having LOS conditions.

arrays the shadow fading and correlation structure become further away from the Toeplitz structure. Comparing the sum-rate achieved in the Kronecker model with the one in the measured channels, we can see that the Kronecker model underestimates the sum-rate, especially for larger arrays. At $E_s/N_0 = 10$ dB, the sum-rate obtained by the Kronecker model with the measured correlation is 4%, 9%, 10% and 12% lower than that in the measured channels, for 5, 32, 64 and 128 antennas, respectively.

Next we look at the situation in the NLOS scenario where the users are located at MS 5. In the angular power spectrum shown in Fig. 7(a), the energy is distributed at larger angles in this scenario, as compared to the two LOS scenarios. Variation in the angular power spectrum along the array can also be observed here. The averaged fading and correlation matrix in Fig. 7(b) becomes more diagonal-dominant. The variation in channel strength is smaller in this scenario, around 7 dB, as shown in Fig. 7(c). The correlation in Fig. 7(d) drops rapidly as the antenna separation increases, which is expected in NLOS conditions. At 2-wavelength separation, the correlation coefficient is already as small as 0.1.

In Fig. 8, we also observe that the measured correlation is closer to the Toeplitz structure in terms of uplink sum-rate, when the array is smaller, but becomes more distinct as the array size grows. At $E_s/N_0 = 10$ dB, the Kronecker model with the Toeplitz-structured correlation achieves 10%, 23%, 25% and 27% higher sum-rate than the model with the measured correlation, for 5, 32, 64 and 128 antennas, respectively. The Kronecker model with the measured correlation again underestimates the measured sum-rate. At $E_s/N_0 = 10$ dB, it gives 12%, 18%, 19% and 20% lower sum-rate, for 5, 32, 64 and 128 antennas, respectively.

In the scenarios discussed above, the users are closely located at the same site. When users are well separated, *e.g.*, at different sites, the fading and correlation properties on the linear array are also quite different from the Toeplitz structure, and the Kronecker model still underestimates the sum-rate in this case. Due to the space limitation, we omit the illustration of the situation where users are well separated.

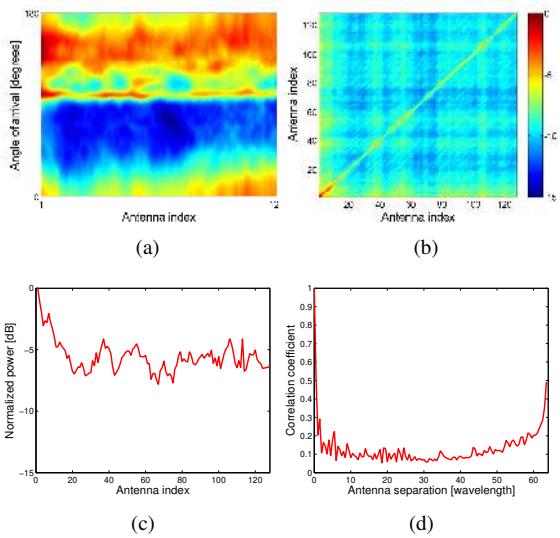

Fig. 7. An NLOS scenario where five users are at MS 5. (a) Angular power spectrum along the linear array. (b) Averaged fading and correlation over subcarriers on the array. (c) Variation in channel strength across the array. (d) Averaged spatial correlation with respect to antenna separation.

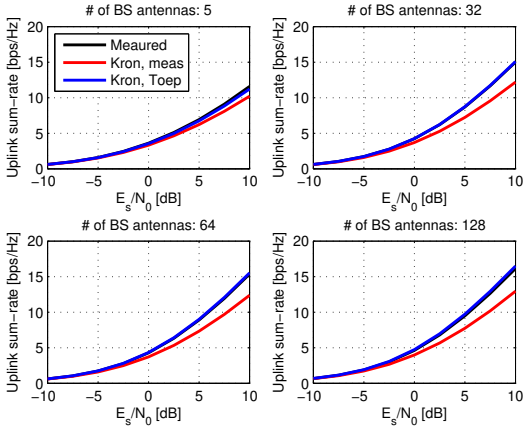

Fig. 8. Comparison of the sum-rates achieved in the measured channels, and in the Kronecker model with the measured and the Toeplitz correlation. The five users are at MS 5 with NLOS conditions.

B. Cylindrical array

The averaged power variation and correlation on the cylindrical array is shown in Fig. 9, for a LOS scenario and an NLOS scenario. The antennas are indexed as follows. The first 64 are vertically-polarized, and the last 64 are horizontally-polarized, antennas pointing in the same direction are ordered after each other and from bottom to top. We can see in Fig. 9 that the power variation and correlation properties are obviously not Toeplitz-structured. This is due to the patch antennas and circular arrangement of the cylindrical array, rather than variation in the propagation channels over a large physical dimension. It indicates that although this array is small in size, the Toeplitz structure is still not suitable. Antenna patterns should be considered when simulating this type of arrays.

V. Summary

Using measured channels, we illustrate the fading and spatial correlation properties on large arrays, in different propagation environments. The study shows that in massive MIMO

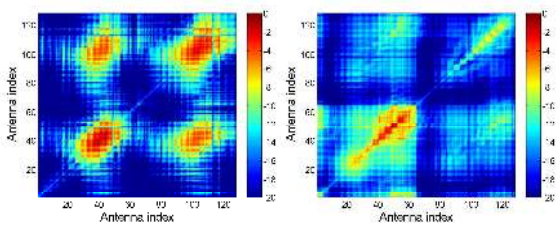

Fig. 9. Averaged correlation matrix over subcarriers with the cylindrical array. (a) A LOS scenario, users at MS 1. (b) An NLOS scenario, users at MS 5.

these properties cannot be characterized well by the Kronecker and Toeplitz assumptions on their correlation, often used successfully for smaller MIMO arrays. Large arrays are highly dependent on their immediate environment, where shadowing and resulting variations along the array play an important role. Channel models that capture the variations in channel strength and spatial correlation across large arrays should be developed specifically for massive MIMO. Future work may include extending the study by using the Weichselberger model [14], which introduces coupling between the transmitter and receiver, and has been shown to be more accurate than the Kronecker model when estimating channel capacity.

References

[1] A. V. Zelst and J. S. Hammerschmidt, "A single coefficient spatial correlation model for multiple-input multiple-output (MIMO) radio channels," in *Proc. URSI XXVIIth General Assembly*, 2002, pp. 1–4.

[2] X. Mestre, J. Fonollosa, and A. Pages-Zamora, "Capacity of MIMO channels: asymptotic evaluation under correlated fading," *IEEE Journal on Selected Areas in Communications*, vol. 21, no. 5, pp. 829–838, June 2003.

[3] F. Rusek, D. Persson, B. K. Lau, E. G. Larsson, T. L. Marzetta, O. Edfors, and F. Tufvesson, "Scaling up MIMO: Opportunities and challenges with very large arrays," *IEEE Signal Processing Magazine*, Jan. 2013.

[4] E. Larsson, O. Edfors, F. Tufvesson, and T. Marzetta, "Massive MIMO for next generation wireless systems," *IEEE Communications Magazine*, vol. 52, no. 2, pp. 186–195, February 2014.

[5] X. Gao, O. Edfors, F. Rusek, and F. Tufvesson, "Massive MIMO in real propagation environments," *IEEE Transactions on Wireless Communications*, 2014, submitted.

[6] X. Gao, F. Tufvesson, O. Edfors, and F. Rusek, "Measured propagation characteristics for very-large MIMO at 2.6 GHz," in *2012 46th Asilomar Conference on Signals, Systems and Computers*, 2012, pp. 295–299.

[7] X. Gao, F. Tufvesson, and O. Edfors, "Massive MIMO channels - measurements and models," in *2013 47th Asilomar Conference on Signals, Systems and Computers*, 2013.

[8] D. Chizhik, J. Ling, P. Wolniansky, R. Valenzuela, N. Costa, and K. Huber, "Multiple-input-multiple-output measurements and modeling in Manhattan," *IEEE Journal on Selected Areas in Communications*, vol. 21, no. 3, pp. 321–331, Apr 2003.

[9] D. shan Shiu, G. Foschini, M. Gans, and J. Kahn, "Fading correlation and its effect on the capacity of multielement antenna systems," *IEEE Transactions on Communications*, vol. 48, no. 3, pp. 502–513, Mar 2000.

[10] S. H. Nelson Costa, *Multiple-Input Multiple-Output Channel Models: Theory and Practice*. Wiley, 2010.

[11] H. Ozcelik, M. Herdin, W. Weichselberger, J. Wallace, and E. Bonek, "Deficiencies of 'Kronecker' MIMO radio channel model," *Electronics Letters*, vol. 39, no. 16, pp. 1209–1210, Aug 2003.

[12] A. Paulraj, R. Nabar, and D. Gore, *Introduction to Space-Time Wireless Communications*. New York, USA: Cambridge University Press, 2008.

[13] A. Molisch, *Wireless Communications*. Wiley-IEEE Press, 2005.

[14] W. Weichselberger, "Spatial structure of multiple antenna radio channels," PhD Thesis, Technischen Universit´at Wien, 2003.